FULL PAPER

Geospace exploration project ERG

Yoshizumi Miyoshi[1]*, Iku Shinohara[2], Takeshi Takashima[2], Kazushi Asamura[2], Nana Higashio[3],
Takefumi Mitani[2], Satoshi Kasahara[4], Shoichiro Yokota[5], Yoichi Kazama[6], Shiang-Yu Wang[6], Sunny W. Y. Tam[7],
Paul T. P. Ho[6], Yoshiya Kasahara[8], Yasumasa Kasaba[9], Satoshi Yagitani[8], Ayako Matsuoka[2], Hirotsugu Kojima[10],
Yuto Katoh[9], Kazuo Shiokawa[1] and Kanako Seki[4]

Abstract

The Exploration of energization and Radiation in Geospace (ERG) project explores the acceleration, transport, and loss of relativistic electrons in the radiation belts and the dynamics for geospace storms. This project consists of three research teams for satellite observation, ground-based network observation, and integrated data analysis/simulation. This synergetic approach is essential for obtaining a comprehensive understanding of the relativistic electron generation/loss processes of the radiation belts as well as geospace storms through cross-energy/cross-regional couplings, in which different plasma/particle populations and regions are strongly coupled with each other. This paper gives an overview of the ERG project and presents the initial results from the ERG (Arase) satellite.

Keywords: The ERG project, The ERG (Arase) satellite, The radiation belts, Geospace

Introduction

The radiation belts consist of energetic charged particle populations that are trapped in the inner magnetosphere. Associated with solar wind disturbances, the outer radiation belt electron population varies considerably. In particular, a decrease in the flux of relativistic electrons is observed during the main phase of geospace storms. The flux then recovers and often significantly increases during the recovery phase of storms (e.g., Nagai 1988; Miyoshi and Kataoka 2005). The identification of mechanisms that drive the flux variations of relativistic electrons in the radiation belts is fundamental and important problem in the solar-terrestrial physics.

There are several plasma and particle populations in the inner magnetosphere. The plasmasphere consists of cold/dense plasma populations, and the ionosphere is the source of the plasmaspheric plasma. The typical energy of the plasmaspheric plasma is less than 1 eV. The typical ring current and plasma sheet energies range from a few keV to about 100 keV, and these populations contribute to the ambient plasma pressure. The typical energies of the radiation belt particles range from a few hundred keV
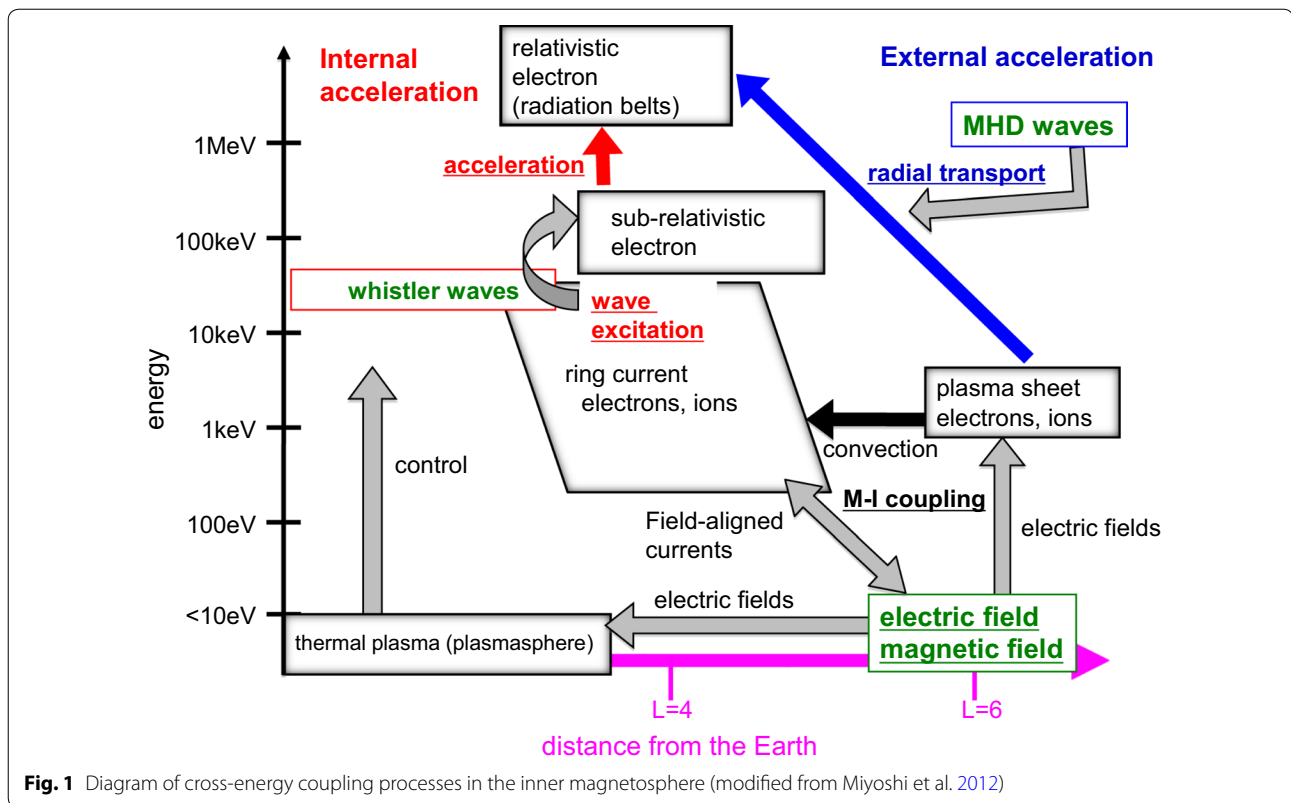
to more than 10 MeV, which are the highest energy population in geospace. Thus, plasma and particle populations with a wide range of energies from a few eV to more than 10 MeV coexist in the inner magnetosphere. Reviews on the inner magnetosphere can be found in several papers (e.g., Ebihara and Miyoshi 2011).

Two different mechanisms have been considered to cause the large flux enhancement of the outer radiation belt electrons. One is an external source process via quasi-adiabatic acceleration, which is the so-called radial diffusion. The other mechanism is an internal acceleration process. Figure 1 shows a diagram of the expected transportation and acceleration mechanisms as a function of the L-shell and energy. In the radial diffusion, i.e., the external source process (blue arrows), the electrons move earthward with increasing energy because of the conservation of the first two adiabatic invariants. The drift resonance with the MHD fast-mode waves is expected to cause the radial transportation of electrons, and the ultra-low frequency (ULF) geomagnetic pulsations of Pc4 and Pc5 are the primary waves that cause the resonance (e.g., Elkington et al. 1999). During the internal acceleration process (red arrows), sub-relativistic electrons are accelerated to MeV energies by whistler mode waves inside the radiation belts (e.g., Summers et al. 1998; Miyoshi et al. 2003; Thorne 2010). In this process,

*Correspondence: miyoshi@isee.nagoya-u.ac.jp
[1] ISEE, Nagoya University, Nagoya 464-8601, Japan
Full list of author information is available at the end of the article

Miyoshi *et al. Earth, Planets and Space* (2018) 70:101

Page 2 of 13

Fig. 1 Diagram of cross-energy coupling processes in the inner magnetosphere (modified from Miyoshi et al. 2012)

the whistler mode waves act as a mediating agent. The waves are generated through the plasma instability of hot electrons and subsequent nonlinear interactions (e.g., Omura et al. 2009), and the energy of the hot electrons transfers to the waves. The waves accelerate sub-relativistic electrons and enhance the relativistic electron flux. The cold plasma density population also contributes to this process because the cold plasma density controls the wave dispersion and resonance conditions. Thus, the cross-energy coupling of different energy plasmas and particle populations via wave–particle interactions plays an important role in the flux enhancements of the radiation belt electrons (Miyoshi et al. 2012, 2016).

There are debates on which external source process and internal acceleration process are important for the large flux enhancement of the outer radiation belt electrons. Phase space density profiles were derived from NASA/Van Allen Probe observations (Mauk et al. 2013) in the October 2012 geospace storm, and it is identified for the first time that the internal acceleration process was dominant during the flux enhancement of MeV electrons (Reeves et al. 2013). It is expected that both the external source and internal acceleration processes are not exclusive, and the dominant processes that cause the large flux enhancements depend on the events (e.g., Reeves et al. 2003). So, long-term observations of the radiation

belts are important to clarify how the external source and internal acceleration processes depend on different geomagnetic and solar wind conditions.

To understand the detailed acceleration and transportation processes, it is necessary to know all parameters that contribute to the accelerations. Electrons over wide energy ranges and electric and magnetic fields with wide frequency ranges are indispensable for understanding these processes. Observations of the ambient plasma density are also necessary. In addition, it is essential to simultaneously evaluate the loss processes in the radiation belts. Several processes contribute to the loss of the radiation belt electrons, escaping into the magnetopause, and the pitch angle scattering into the atmosphere because of the whistler mode waves and electromagnetic ion cyclotron (EMIC) wave–particle interactions (e.g., Turner et al. 2012).

Here, we describe the importance of multi-point observations in the inner magnetosphere. Several kinds of plasma waves play a key role for accelerations and loss of electrons in the radiation belt electrons. Whistler mode chorus waves accelerate relativistic electrons on the dawnside outside the plasmapause, whereas whistler mode hiss waves cause pitch angle scattering inside the plasmasphere. EMIC waves cause a strong scattering of MeV electrons (e.g., Miyoshi et al. 2008), which are

Miyoshi *et al. Earth, Planets and Space* (2018) 70:101

Page 3 of 13

mainly observed on the dusk and noon sides (e.g., Shprits et al. 2008a, b). These wave–particle interactions often occur simultaneously at different local times and radial distances.

Moreover, the causes and consequences of the processes are often observed at different locations. For example, the pitch angle scattering with whistler mode waves occurs in the magnetosphere, while the resultant precipitations are observed at ionospheric altitudes. In this example, it is possible to identify the causal relationship using conjugate observations between satellite and ground-based instruments. Thus, multi-point observations by multiple satellites and conjugate observations with ground-based observations are necessary for understanding the dynamics of the inner magnetosphere.

In addition to the observations, simulation studies are helpful for investigating the cause and consequence of phenomena and identify the relative role of each mechanism, because different physical processes work simultaneously and strongly couple with each other. Comprehensive simulations and modeling for the whole inner magnetosphere including different physical processes are necessary to identify the role of each process.

In order to elucidate the flux enhancement and loss processes of the relativistic electrons of the outer radiation belt as well as the dynamics of geospace storms through cross-energy and cross-regional couplings, the Exploration of energization and Radiation in Geospace (ERG) project has been organized. The following teams are involved in the ERG project: the satellite observation team, ground-based network observation team, and integrated data analysis/simulation team. The synergetic approach with these teams provides a comprehensive view of the radiation belts and inner magnetosphere for geospace storms. The main science questions of this project are as follows:

1. What are the dominant processes to cause the large flux enhancement of relativistic electrons of the outer radiation belt?
2. How do wave–particle interactions accelerate the relativistic electrons of the outer radiation belt?
3. What are the dominant loss processes for the relativistic electrons of the outer radiation belt?

In this paper, we describe an overview of the ERG project and show the initial observation results from the ERG (Arase) satellite.

ERG (Arase) satellite
Overview
The ERG (Arase) satellite was developed by the Institute of Space and Astronautical Science (ISAS)/Japan Aerospace Exploration Agency (JAXA), and nine science instruments were developed at ISAS/JAXA as well as several universities and institutes in Japan and Taiwan. The satellite was successfully launched by the Epsilon launch vehicle from the Uchinoura Space Center of JAXA on December 20, 2016. Table 1 presents the specifications of the spacecraft, and Fig. 2 shows an image of the satellite in the radiation belts.

The ERG satellite is designed to be Sun oriented and spin stabilized with a rotation rate of 7.5 rpm. The apogee altitude is ~ 32,000 km, and the perigee altitude is ~ 400 km, so that the satellite explores the entire region of the radiation belts. The inclination angle of the satellite orbit is about 31°, and therefore, the satellite sometimes covers a wide L-shell region up to about 10–11 when the apogee altitudes are at large magnetic latitudes (MLATs). Details of the satellite system have been introduced by other papers (Takashima et al. 2018; Nakamura et al. 2018).

Figure 3 shows the orbit of the ERG satellite for four different seasons in the equatorial plane and meridional plane. The initial magnetic local time (MLT) of the apogee altitude was nine, and the apogee MLT then shifted from dawn to dusk through the night. Because the critical phase and commissioning phase operation took 3 months, regular observations with full operation of all the instruments started at 0600 MLT in March, 2017. The lines of the apogee progress in local time at a rate of approximately 260° per year in the clockwise direction (looking down from the north).

Immediately after the beginning of regular observations in March 2017, the ERG satellite observed the inner magnetosphere near the magnetic equator at the heart of the outer radiation belt ($L = 4 - 6$) on the morning side (black curves). Because the generation of chorus waves is typically expected in this area (e.g., Shprits et al. 2008a, b), the science objectives on the morning side were the chorus wave–particle interactions.

The apogee MLT shifted to the night side during the summer of 2017 (blue curve) and then the dusk side

Table 1 Outline of the ERG satellite

Launch vehicle	Epsilon-2
Launch	December 20, 2016
Weight (kg)	~ 350
Size (m)	1.5 × 1.5 × 1.7
Orbit (km)	~ 32,000 (Apogee altitude), ~ 400 (Perigee altitude)
Inclination angle (°)	31
Orbit period (min)	~ 570
Science payload	Nine scientific instruments (see Table 2)
Appendages	Two pairs of 5-m masts, two pairs of 30-m tip-to-tip wire antennas

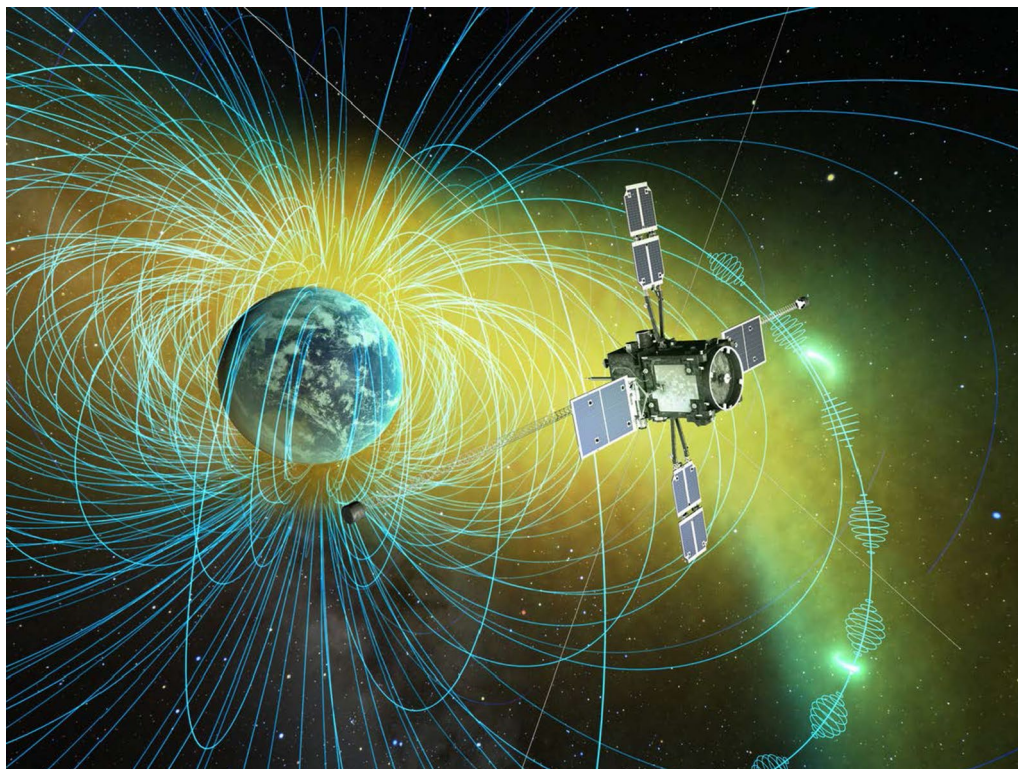Miyoshi *et al. Earth, Planets and Space* (2018) 70:101

Page 4 of 13

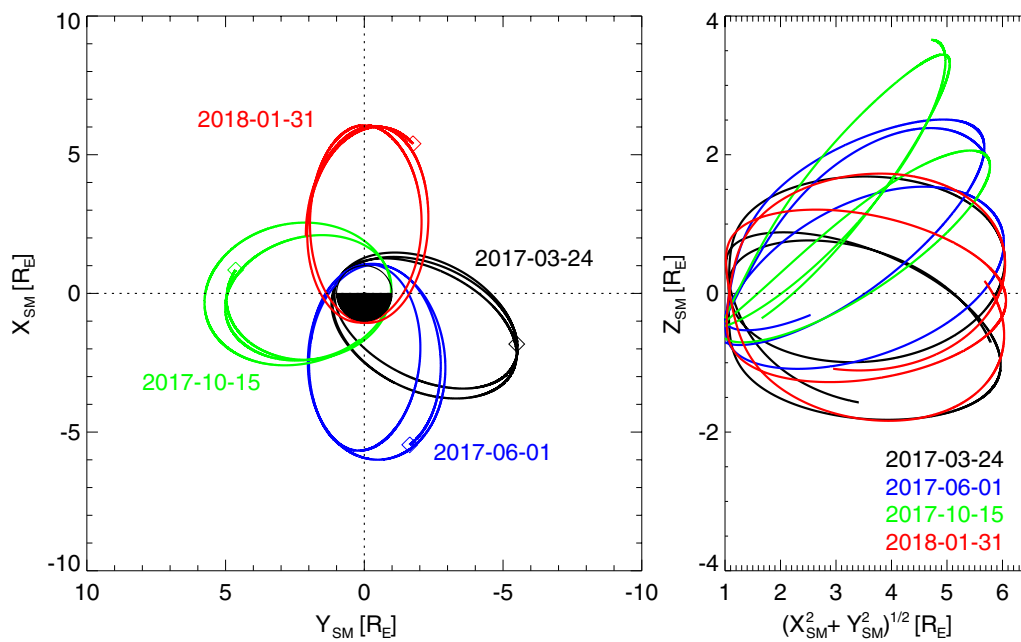**Fig. 2** Image of the ERG satellite observations in the geospace

Fig. 3 Sample orbits of the ERG satellite. Black: March 24, 2017, Blue: June 1, 2017, Green: October 15, 2017, and Red: January 31, 2018

Miyoshi *et al. Earth, Planets and Space* (2018) 70:101

Page 5 of 13

during the fall of 2017 (green curve). During this period, the apogee MLATs were about 30°–40° and the ERG satellite covered a wider *L*-shell region up to $L \sim 9$ and often observed not only the plasma sheet and inner magnetosphere but also the plasma sheet boundary layer and tail lobes near the apogee.

Then, the apogee MLT moved to the noon side (red curve). The ERG satellite covered around the magnetic equator at the apogee altitudes. Because the EMIC waves are typically observed on the dusk and noon sides (e.g., Shprits et al. 2008a, b), the wave–particle interactions between the EMIC waves and ring current ions as well as the relativistic electrons in the outer radiation belt were the primary science objectives during this period.

Science instruments

Comprehensive observations of the inner magnetosphere for plasma/particles and fields/waves are important for understanding the role of cross-energy coupling for the dynamics of relativistic electrons as well as geospace storms. Nine instruments are installed on the ERG satellite, as shown in Fig. 4 and Table 2.

Figure 5 shows the energy and frequency coverages of these instruments. To measure electrons over a wide range of energies, including warm electrons, hot electrons in the plasma sheet and ring current, and sub-relativistic and relativistic electrons of the radiation belts, four instruments are installed: low-energy particle experiments-electron analyzer (LEP-e) (Kazama et al. 2017), medium-energy particle experiments-electron analyzer (MEP-e) (Kasahara et al. 2018a), high-energy electron

Fig. 4 Configuration of science instruments onboard the ERG satellite

Table 2 List of science instruments onboard ERG satellite

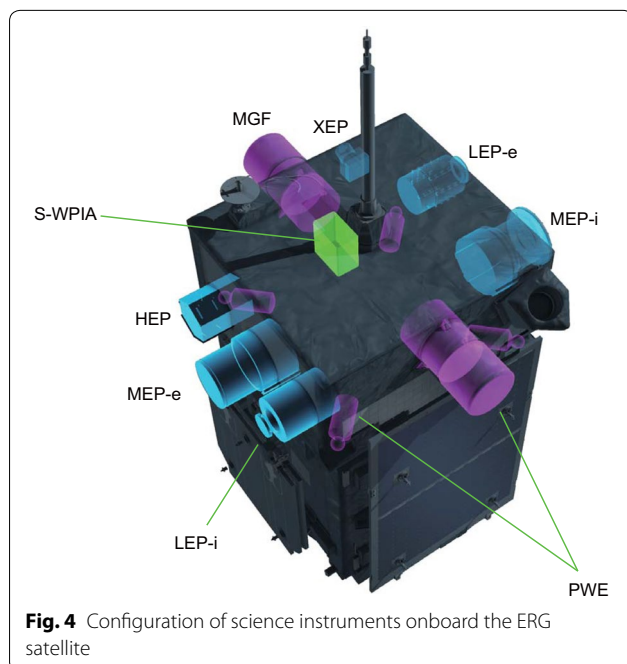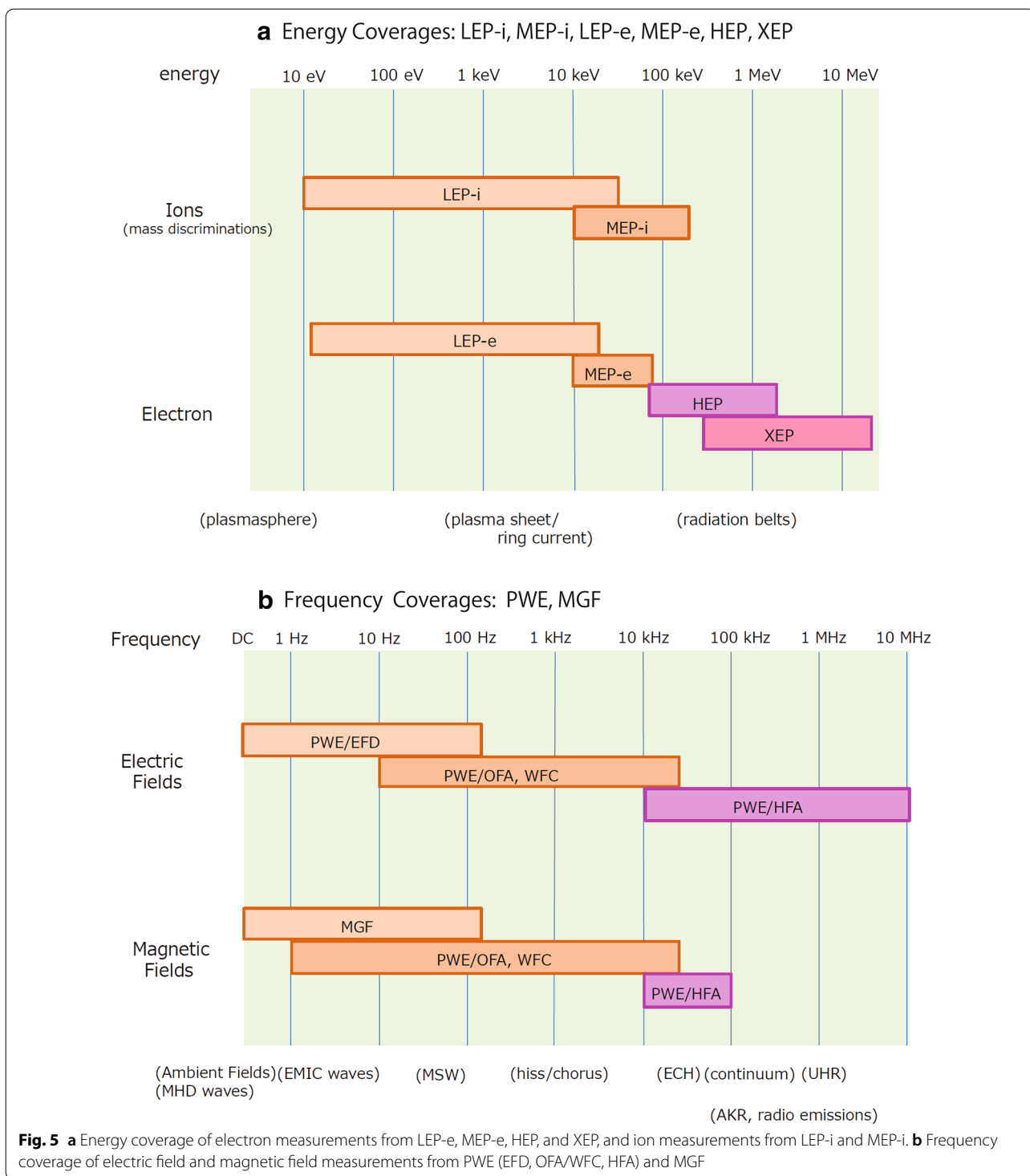| Instrument		Measurement
LEP-e	Low-energy particle experiments–electron analyzer	19 eV–20 keV (electron)
MEP-e	Medium-energy particle experiments–electron analyzer	7–87 keV (electron)
HEP	High-energy electron experiments	
	HEP-L	70 keV–1 MeV (electron)
	HEP-H	0.7–2 MeV (electron)
XEP	Extremely high-energy electron experiment	400 keV–20 MeV (electron)
LEP-i	Low-energy particle experiments–ion mass analyzer	10 eV/q–25 keV/q (ions) (mass discriminations)
MEP-i	Medium-energy particle experiments–ion mass analyzer	10–180 keV/q (ions) (mass discriminations)
PWE	Plasma wave experiment	
	Electric field detector (EFD)	DC–512 Hz (electric field waveform and spectrum)
	Onboard frequency analyzer (OFA)	10 Hz–20 kHz (electric field spectrum) 1 Hz–20 kHz (magnetic field spectrum)
	Waveform capture (WFC)	10 Hz–20 kHz (electric field waveform) 1 Hz–20 kHz (magnetic field waveform)
	High-frequency analyzer (HFA)	10 kHz–10 MHz (electric field spectrum) 10 kHz–100 kHz (magnetic field spectrum)
MGF	Magnetic field experiment	DC–256 Hz (magnetic field waveform)
S-WPIA	Software-type wave–particle interaction analyzer	Phase between waves and particles

experiment (HEP) (Mitani et al. 2018), and extremely high-energy electron experiment (XEP). In parallel, to measure the warm ions and energetic ions of the plasma sheet and ring current with mass discrimination, two instruments are installed: low-energy particle experiments-ion analyzer (LEP-i) (Asamura et al. 2018) and medium-energy particle experiments-ion mass analyzer (MEP-i) (Yokota et al. 2017). The energy ranges of the instruments are designed to overlap each other to provide a continuous energy spectrum for various plasma/particle populations in the inner magnetosphere.

From these instruments, the ERG satellite measures electrons with a wide range of energies, from 19 eV to 20 MeV. Moreover, not only the pitch angle distributions but also the three-dimensional distribution function data are obtained up to 2 MeV in each spin period from the LEP-e/MEP-e/HEP instruments. In the wave–particle interactions, low-energy electrons contribute to the

Miyoshi *et al. Earth, Planets and Space* (2018) 70:101

Page 6 of 13

a Energy Coverages: LEP-i, MEP-i, LEP-e, MEP-e, HEP, XEP

b Frequency Coverages: PWE, MGF

Fig. 5 a Energy coverage of electron measurements from LEP-e, MEP-e, HEP, and XEP, and ion measurements from LEP-i and MEP-i. **b** Frequency coverage of electric field and magnetic field measurements from PWE (EFD, OFA/WFC, HFA) and MGF

generation of plasma waves through anisotropies in the distribution function, and the LEP-e/MEP-e measurements identify the variations in the distribution function associated with the wave–particle interactions.

The LEP-i and MEP-i measure ions from 10 eV/q to 180 keV/q with mass discrimination. Ion species are discriminated using the time-of-flight method. These ion observational data are used to identify the free energy source to generate EMIC waves and magnetosonic mode

Miyoshi *et al. Earth, Planets and Space* (2018) 70:101

Page 7 of 13

waves (equatorial noise) (e.g., Kasahara et al. 1994; Ma et al. 2014). The data are also used to study the ring current evolution and variations of ion compositions, which are necessary for understanding how ion distributions modify the magnetic field configuration during geospace storms (e.g., Nose et al. 2005).

The plasma wave experiment (PWE) observes electric fields in the frequency range from DC to 10 MHz and magnetic fields in the frequency range from a few Hz to 100 kHz (Kasahara et al. 2018c). The electric field component is measured by two pairs of wire dipole antennas with a tip-to-tip length of 30 m, and the magnetic field component is measured using three-axis search coils (Ozaki et al. 2018). The PWE consists of four subcomponents: an electric field detector (EFD) (Kasaba et al. 2017), onboard frequency analyzer (OFA), waveform capture (WFC) (Kasahara et al. 2018c; Matsuda et al. 2018), and high-frequency analyzer (HFA) (Kumamoto et al. 2018). The EFD produces low-frequency waveform data with a sampling frequency of 512 Hz and the spacecraft potential. The EFD measures the ambient electric fields and ULF waves as well as the EMIC waves. The OFA produces the power spectrum as well as the spectrum matrix for both electric fields and magnetic fields from 10 Hz to 20 kHz. The time resolutions of the power spectrum and spectrum matrix are nominally 1 and 8 s, respectively, while the possible time resolutions are 0.5–4 and 4–32 s, respectively. The WFC observes the raw waveforms of the electric/magnetic fields with 65-kHz sampling for the chorus burst mode and 1-kHz sampling for the EMIC burst mode. As the data size of the WFC is often too large to download to the ground without any data reduction, the OFA data are also used to select the WFC data period for downloading to the ground. The HFA produces the power spectra for the electric fields (10 kHz–10 MHz) and magnetic fields (10–100 kHz), and the data are used to measure the upper hybrid resonance (UHR) waves and several radio waves such as auroral kilometric radiation (AKR) and type III solar radio bursts. Because the UHR frequency is a function of the ambient electron density, the HFA provides the ambient plasma density along the orbit.

The magnetic field experiment (MGF) measures magnetic fields from DC to several tens of Hz (the sampling frequency is 256 Hz). That is, the MGF observes the ambient magnetic fields, i.e., the background field strength and direction, ULF waves, and EMIC waves (Matsuoka et al. 2018). The field direction error of the MGF measurements is less than 1°, so it is possible to analyze the field distortions in detail due to the ring current and field-aligned current.

To understand energy exchange processes between electrons and waves through wave–particle interactions, a software-type wave–particle interaction analyzer (S-WPIA) is installed on the satellite (Katoh et al. 2018; Hikishima et al. 2018). The phase difference between the electric/magnetic fields of the plasma waves and gyrating electrons determines whether the waves accelerate the electrons, or the electrons generate the waves. The S-WPIA system calculates the phase difference with a time resolution of 10 μs under the cooperation of the MEP-e/HEP/XEP, PWE, and MGF instruments. The S-WPIA realizes a new observation to identify unambiguously how energy conversion occurs in the wave–particle interactions.

The ERG satellite provides not only the data mentioned above but also quasi-real time space weather data. The space weather data include datasets from the XEP, HEP, and MGF instruments. These data are downloaded to the ground immediately after the observation and are displayed on the webpage of JAXA. These data are not fully calibrated, so it is not always possible to use the quantitative analyses, but the data are useful for monitoring the current space environment.

Ground-network observations and integrated data analysis/simulation

In addition to the ERG satellite observations, the project consists of the ground-network observations and integrated data analysis/simulation teams. Conjugate observations between the ERG satellite and multi-point ground-based network are important for a comprehensive understanding of geospace because the ground-based network observations provide the data at different MLTs and invariant latitudes (Shiokawa et al. 2017). For example, Super Dual Aurora Radar Network (SuperD-ARN) radars provide the data for convection electric fields and ULF pulsations at different MLTs and latitudes. Magnetometer networks provide temporal-spatial distributions of EMIC (Pc1) and Pc3–Pc5 ULF waves as well as ionospheric currents. Very low frequency (VLF)/extremely low frequency (ELF) receivers observe the chorus/hiss waves. The optical imagers observe electron and proton auroras, which indicate precipitations of electrons and ions from a few hundred eV to a few tens of keV. Riometers observe cosmic noise absorption, which is a manifestation of tens of keV electron precipitations. The standard radio wave observations provide information about disturbances in the D-layer, which are proxies for sub-relativistic/relativistic electron precipitations. These networks of optical imagers, riometers, and standard radio wave observations can be used to specify the spatial location and extent of precipitating particles and waves. The incoherent scatter radar such as European Incoherent Scatter Radar (EISCAT) provides the energy spectrum of precipitating electrons.

Miyoshi *et al. Earth, Planets and Space* (2018) 70:101

Page 8 of 13

In order to investigate the physical processes quantitatively and reveal the relative role of each process, integrated data analyses with the numerical simulations are indispensable (Seki et al. 2018). The multi-point observations of the ERG satellite and ground-based observations provide a macroscopic view of geospace, which can be compared to the global simulation for the inner magnetosphere, e.g., the evolution of the plasmasphere, ring current, and radiation belts. In contrast, microscopic wave–particle interactions can also be compared with the detailed simulations of the wave–particle interactions (e.g., Katoh and Omura 2007; Hikishima et al. 2009; Saito et al. 2012).

ERG science center

The raw data acquired from the satellite are archived at ISAS. After the data evaluation and necessary processing to generate level-1 data by the instrument teams, level-2 data are generated at the ERG science center (Miyoshi et al. 2018). Level-3 data are generated by combining with the data from several instruments. For example, the electron density along the satellite orbit is level-3 data, which are generated from the UHR frequency measured by the PWE/HFA and the electron gyrofrequency measured by the MGF. Level-4 data are the phase space densities of electrons and ions, which are generated with the inter-calibrated data between different particle instruments. All science data files are distributed from the ERG science center.

In order to realize the integrated data analyses using not only the ERG satellite data but also the ground-based data, other satellite data, and simulation data, the data format and data analysis tools are important. All observation data from the ERG project are archived in the Common Data Format (CDF) that is a common format for the space physics community. The Space Physics Environment Data Analysis System (SPEDAS) (Angelopoulos 2008) is used for the data analysis software in the ERG project, which involves several Interactive Data Language (IDL) programs and is commonly used in the space physics community. The ERG science center developed the SPEDAS plug-in programs for the ERG project, and users can download and manipulate the CDF files of the ERG project using the plug-in programs. Because SPEDAS includes many plug-in programs for not only the ERG project but also other satellites and ground-based observations, users can readily access and analyze different kinds of datasets.

Initial observations

Here, we present the initial observation results from the ERG satellite. Note that the electric field intensity from the PWE instrument in this paper is calculated under the assumption of theoretical antenna capacitance in vacuum to the impedance of the electric field sensors (Kasahara et al. 2018c). Figure 6 shows a summary plot for all instrumental data from the ERG satellite on April 9, 2017. Moderate geomagnetic activity is recorded. The minimum Dst index on this day is − 25 nT. As shown in panel (m), a series of substorms are observed before 17:00 UT, and then, the geomagnetic activity decreases. During this period, the apogee MLT of the satellite is approximately 04:00 MLT.

Panels (a), (b), (c), and (d) present frequency-time diagrams of the PWE/HFA, PWE/OFA (electric fields), PWE/OFA (magnetic fields), and PWE/EFD, respectively. These instruments cover the frequency ranges from DC to 10 MHz. The two lines in panels (a), (b), and (c) indicate the local electron gyrofrequency and the half gyrofrequency derived from the MGF measurements.

In panel (a), emissions of several kinds of plasma waves and radio waves are observed. AKR is observed at a few hundred kHz, and the UHR emissions above the electron gyrofrequency are almost always observed along the orbit. As the PWE/HFA covers wide frequency up to 10 MHz, the satellite observes the UHR emissions during the whole orbit. Using the frequency of the UHR emissions, it is possible to estimate the electron density from the magnetosphere to the topside ionosphere.

In panels (b) and (c), chorus waves at a few hundred Hz to a few kHz are detected outside the plasmapause where the ambient density is low, and both lower-band and upper-band chorus waves are sometimes clearly observed. There are several periods when the frequency of chorus emissions is relatively low compared to the local half gyrofrequency because the satellite traverses off the equatorial plane. Inside the plasmapause, whistler mode hiss waves are observed. Panel (d) presents a frequency-time diagram of the low-frequency electric fields covering the ULF and ELF ranges. Several electrostatic waves are observed, and the banded emissions at 70 Hz at about 23:00 UT are magnetosonic mode waves (equatorial noise).

Panels (e), (f), (g), and (h) present energy-time diagrams of the XEP, HEP, MEP-e, and LEP-e instruments. Note that the color bar indicates the count for the XEP, HEP, and LEP-e, and the flux for the MEP-e. Wide-energy electron measurements are achieved from 17 eV to 20 MeV. The energy-time diagram of the XEP shows the outer radiation belt population. The peak of the count is $L \sim 4.5$, and a clear inner boundary of the outer radiation belt is observed at $L \sim 3.3$ in every path. Note that the L-value in this paper is the McIlwain L (McIlwain 1961) derived from the International Geomagnetic Reference Field model.

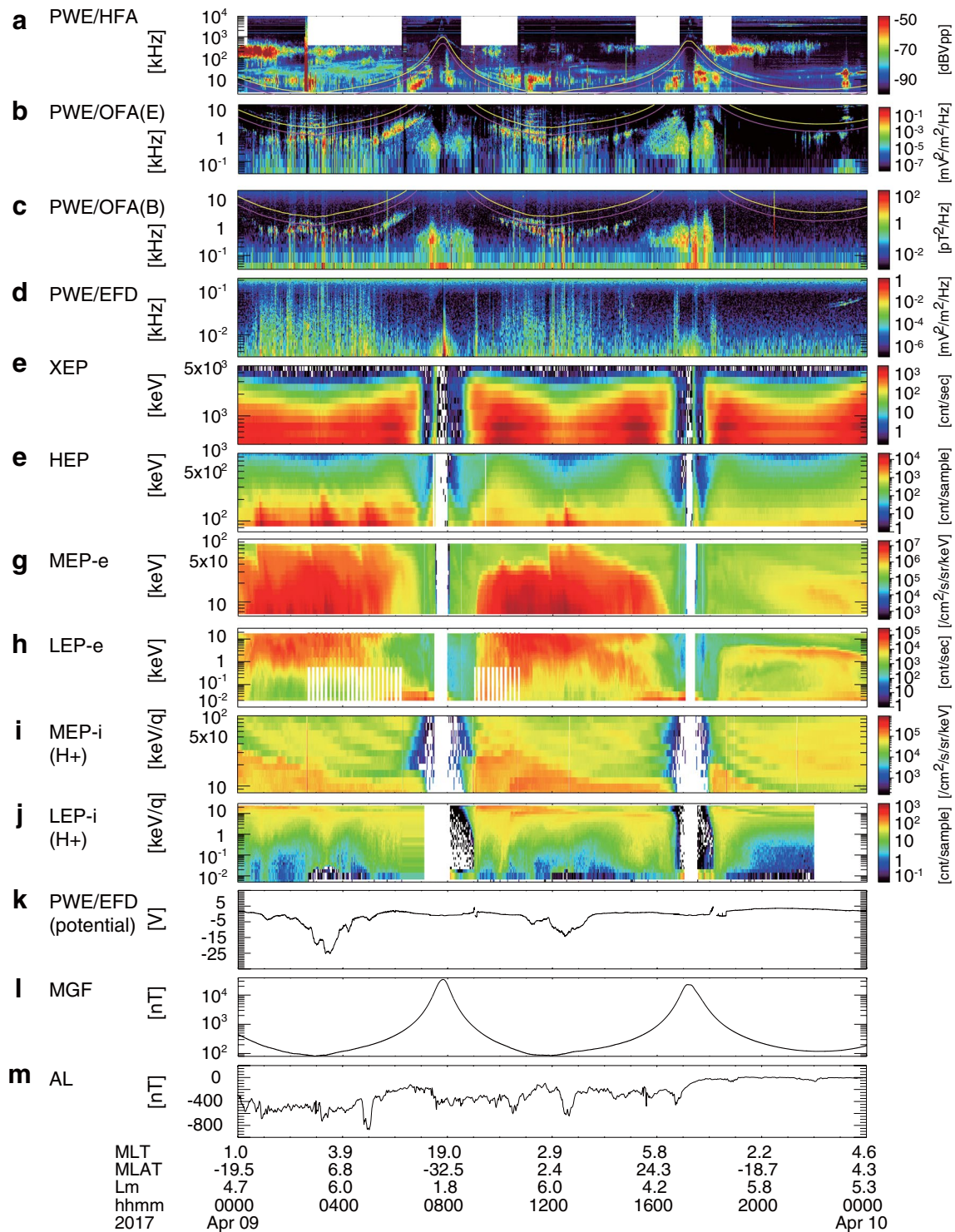Miyoshi *et al. Earth, Planets and Space* (2018) 70:101

Page 9 of 13

Fig. 6 Integrated plots for the ERG satellite observations on April 9, 2017. **a** Frequency-time diagrams of **a** PWE/HFA, **b** PWE/OFA (electric field), **c** PWE/OFA (magnetic field), and **d** PWE/EFD. Energy-time diagrams of electrons from **e** 400 keV to 5 MeV by XEP, **f** 70–1000 keV by HEP-L, **g** 7–87 keV by MEP-e, and **h** 17 eV to 20 keV by LEP-e. Energy-time diagrams of protons from **i** 5–110 keV/q by MEP-i and **j** 10 eV/q to 25 keV/q by LEP-i. **k** Satellite potential measured by PWE/EFD, **l** ambient magnetic field measured by MGF, and **m** AL index. Yellow and magenta lines in panels **a**–**c** indicate the electron gyrofrequency and the half electron gyrofrequency derived from the MGF observations at the satellite position

Miyoshi *et al. Earth, Planets and Space* (2018) 70:101

Page 10 of 13

The LEP-e, MEP-e, and HEP clearly detect dynamical variations of electrons from a few hundred eV to a few tens of keV inside the outer radiation belt. The white blank periods for the LEP-e measurements in panel (h) correspond to the loss-cone measurements (Kazama et al. 2017). During this period, the satellite performs conjugate observations with ground instruments, and the LEP-e instruments measure the electron flux variations inside the loss cone to identify the precipitation of auroral electrons. Sometimes, these three instruments observe signatures of injections in which energy dispersions are observed from a few keV to a few hundred keV electrons. It is expected that electrons injected from the night side drift to the morning side where the satellite observes them.

Panels (i) and (j) present energy-time spectrograms of protons by the MEP-i and LEP-i. Note that the color bar indicates the count for the LEP-i and the flux for the MEP-i. As the satellite is on the dawn side, the flux of ions is relatively small, but energy-dependent structures are clearly detected. Inside the plasmapause, low-energy ions below 1 keV are detected.

Panel (k) shows the time variations of the satellite potential measured with the PWE/EFD. The negative charging of the satellite is observed. Panel (l) shows the magnetic field observed by the MGF. The intensity of the magnetic field is less than 100 nT near the apogee, while the intensity is larger than 35,000 nT near the perigee. During this period, the MGF measures variations in the magnetic field along the orbit, e.g., deformations of the magnetic field and ULF pulsations.

As shown in panel (m), several substorm activities are observed during this period. Associated with the substorm activities from 00:00 to 14:00 UT, injections of electrons are detected with the LEP-e, MEP-e, and HEP. As seen in panels (b) and (c), intense chorus emissions are associated with the injections. Moreover, the potential clearly decreases, as shown in panel (k), during the injections of hot electrons and sub-relativistic electrons, indicating satellite charging during this period.
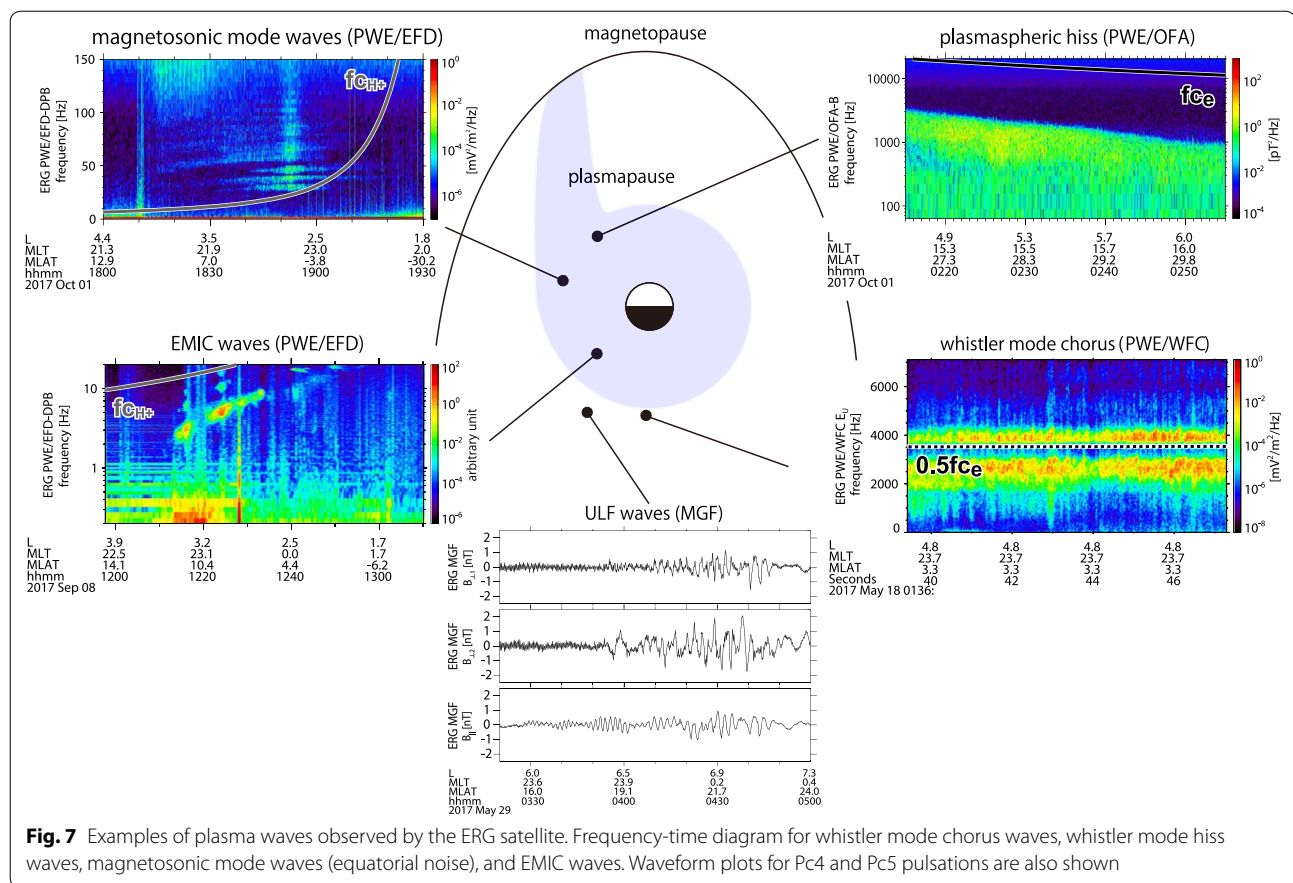
After 17:00 UT, the geomagnetic activities decrease and no substorms are observed. Relativistic electrons of the outer radiation belt do not change significantly compared with previous periods, as shown by the XEP and HEP measurements [panels (e) and (f), respectively]. In contrast, the low-energy electron fluxes decrease, as shown in the MEP-e and LEP-e measurements. Especially, the tens of keV electrons measured with the MEP-e do not exhibit any significant variations during this period. Chorus waves are not observed in panels (b) and (c) because of the absence of free energy to generate chorus waves.

Figure 7 shows examples for various kinds of plasma waves observed by the PWE/OFA, PWE/WFC, PWE/

EFD, and MGF at different MLTs and radial distances. As shown in Fig. 7, the ERG satellite often observes whistler mode chorus waves outside the plasmapause, while the ERG satellite observes whistler mode hiss waves inside the plasmapause. Magnetosonic mode waves (equatorial noise) and EMIC waves are observed inside and outside the plasmapause. Waveforms of Pc4 and Pc5 pulsations observed by the MGF are shown. Both PWE/EFD and MGF always measure waveform of Pc4 and Pc5 pulsations and EMIC waves, while PWE/WFC measures waveform for whistler mode waves and magnetosonic mode waves intermittently as burst observations. Since the operation time of PWE/WFC is limited due to the data recorder volume and the downlink rate to the ground (Takashima et al. 2018; Miyoshi et al. 2018), the burst observations are scheduled by considering the possible generation regions of waves and periods for conjugate observations with the ground-based observations and other satellites such as Van Allen Probes.

Conjugate burst observations between the ERG satellite and Van Allen Probes have been operated since June, 2017, and whistler mode chorus and hiss waves as well as lightning whistlers were simultaneously observed by both satellites at almost same *L*-shell but different magnetic latitudes. The ERG satellite operates burst observations to obtain waveform continuously with a 65-kHz sampling and the maximum duration of 40 min. From these observations, it becomes possible to investigate temporal and spatial variations of fine structure of the frequency spectrum of not only whistler mode chorus waves outside the plasmapause but also long duration whistler mode hiss waves inside the plasmapause. Temporal and spatial evolutions of these waves have been studied using these conjugate data. Further conjugate burst observations between the ERG satellite and other satellites will be planned to provide detailed information of generation and propagations of plasma waves in the inner magnetosphere.

Conjugate observations between the ERG satellite and ground-based network stations have been also operated. Simultaneous ground-satellite observations with several ground-based instruments such as high-speed optical cameras, VLF antennas, and the EISCAT radar have been realized. From the conjugate observation on March 27, 2017, one-to-one correspondences were identified among temporal variations of whistler mode chorus bursts, flux modulations of tens keV electrons inside the loss cone from the ERG satellite observation, and luminosity of the pulsating aurora from the ground-based observation, which is a direct evidence that the pitch angle scattering by whistler mode chorus bursts causes luminosity modulations of the pulsating aurora (Kasahara et al. 2018b). Since the ground-network observations provide the data

Miyoshi *et al. Earth, Planets and Space* (2018) 70:101

Page 11 of 13

Fig. 7 Examples of plasma waves observed by the ERG satellite. Frequency-time diagram for whistler mode chorus waves, whistler mode hiss waves, magnetosonic mode waves (equatorial noise), and EMIC waves. Waveform plots for Pc4 and Pc5 pulsations are also shown

at different MLTs and the invariant latitudes (Shiokawa et al. 2017), these observations are complementary to the satellite observations and important to understand global phenomena in the inner magnetosphere. We will plan coordinated observations to take advantage of the most of merits of multi-point observations.

Summary

The ERG project was designed for understanding the energetic electron variations of the radiation belts and geospace storms. The ERG satellite was launched in December 2016 and started full-operation observations on March 24, 2017.

During solar cycle 24, several geospace satellites operate in the inner magnetosphere. The NASA Van Allen Probes explore the radiation belts and the inner magnetosphere. The NASA THEMIS (Angelopoulos 2008) and MMS (Burch et al. 2016) observe the magnetotail as well as the dayside magnetosphere. In addition, Geotail, Cluster, and other satellites operate in geospace. The ERG satellite has joined the international fleet of satellites and collaborated with them as well as with ground-based observations. The ERG project contributes to the comprehensive understanding of geospace with the international collaborations.

The ERG satellite has begun observations. The ERG project will lead to significant advances in the identification of the physical processes causing variations in the radiation belts and geospace storms, and in providing new insight into the cross-energy and cross-regional coupling processes.

Authors' contributions
YM is the project scientist of the ERG project and the lead author of this article. IS is the project manager. TT is the mission manager. KA is the leader of the mission team and PI of LEP-i. NH is the PI of XEP. TM is the PI of HEP. SK is the PI of MEP-e. SY is the PI of MEP-i. SYW is the project manager, SWYT is the project scientist, and Y. Kazama is the project engineer, and PTPH is the PI of LEP-e. Y. Kasahara is the PI of PWE. Y. Kasaba and SY are co-PI of PWE. AM is the PI of MGF. HK is the PI of SWPIA and co-PI of PWE. Y. Katoh is the co-PI of SWPIA. K. Shiokawa is the PI of the ERG-ground network observations team. K. Seki is the PI of the integrated data analysis/simulation team. All authors read and approved the final manuscript.

Author details
[1] ISEE, Nagoya University, Nagoya 464-8601, Japan. [2] ISAS, JAXA, Sagamihara 252-0222, Japan. [3] RDD, JAXA, Tsukuba 305-8505, Japan. [4] The University of Tokyo, Tokyo 113-8654, Japan. [5] Osaka University, Toyonaka 560-0043, Japan. [6] ASIAA, Taipei 10617, Taiwan, ROC. [7] National Cheng Kung University, Tainan 70101, Taiwan, ROC. [8] Kanazawa University, Kanazawa 920-1192, Japan. [9] Tohoku University, Sendai 980-8578, Japan. [10] RISH, Kyoto University, Uji 611-0011, Japan.

Miyoshi *et al. Earth, Planets and Space* (2018) 70:101

Page 12 of 13

Publisher's Note

Springer Nature remains neutral with regard to jurisdictional claims in published maps and institutional affiliations.

References

Angelopoulos V (2008) The THEMIS mission. Space Sci Rev. https://doi.org/10.1007/s11214-008-336-1

Asamura K, Kazama Y, Yokota S, Kasahara S, Miyoshi Y (2018) Low-energy particle experiments-ion mass analyzer (LEPi) onboard the ERG (Arase) satellite. Earth Planets Space 70:70. https://doi.org/10.1186/s40623-018-0846-0

Burch JL, Moore TE, Torbert RB, Giles BL (2016) Magnetospheric multiscale overview and science objectives. Space Sci Rev. https://doi.org/10.1007/s11214-015-064-9

Ebihara Y, Miyoshi Y (2011) Dynamic inner magnetosphere: a tutorial and recent advances. In: Liu W, Fujimoto M (eds) The dynamic magnetosphere. Springer, Berlin. https://doi.org/10.1007/978-94-007-0501-2_9

Elkington SR, Hudson MK, Chan AA (1999) Acceleration of relativistic electrons via drift-resonant interaction with toroidal-mode Pc-5 ULF oscillations. Geophys Res Lett 26:3273–3276

Hikishima M, Yagitani S, Omura Y, Nagano I (2009) Full particle simulation of whistler mode rising chorus emissions in the magnetosphere. J Geophys Res. https://doi.org/10.1029/2008ja013625

Hikishima M, Kojima H, Katoh Y, Kasahara Y, Kasahara S, Mitani T, Higashio N, Matsuoka A, Miyoshi Y, Asamura K, Takashima T, Yokota S, Kitahara M, Matsuda S (2018) Data processing in software-type wave–particle interaction analyzer on board the Arase satellite. Earth Planets Space 70:80. https://doi.org/10.1186/s40623-018-0856-y

Kasaba Y, Ishisaka K, Kasahara Y, Imachi T, Yagitani S, Kojima H, Matsuda S, Shoji M, Kurita S, Hori T, Shinbori A, Teramoto M, Miyoshi Y, Nakagawa T, Takahashi N, Nishimura Y, Matsuoka A, Kumamoto A, Tsuciya F, Nomura R (2017) Wire probe antenna (WPT) and electric field detector (EFD) of plasma wave experiment (PWE) aboard the Arase satellite: specifications

and initial evaluation results. Earth Planets Space 69:174. https://doi.org/10.1186/s40623-017-0760-x

Kasahara Y, Kenmochi H, Kimura I (1994) Propagation characteristics of the ELF emissions observed by the satellite Akebono in the magnetic equatorial region. Radio Sci. https://doi.org/10.1029/94rs00445

Kasahara S, Yokota S, Mitani T, Asamura K, Hirahara M, Shibano Y, Takshima T (2018a) Medium-energy particle experiments-electron analyzer (MEP-e) for the exploration of energization and radiation in geospace (ERG) mission. Earth Planets Space 70:69. https://doi.org/10.1186/s40623-018-0847-z

Kasahara S, Miyoshi Y, Yokota S, Mitani T, Kasahara Y, Matsuda S, Kumamoto A, Matsuoka A, Kazama Y, Frey HU, Angelopoulos V, Kurita S, Keika K, Seki K, Shinohara I (2018b) Pulsating aurora from electron scattering by chorus waves. Nature 556:7692. https://doi.org/10.1038/nature25505

Kasahara Y, Kasaba Y, Kojima H, Yagitani S, Ishisaka K, Kumamoto A, Tsuchiya F, Ozaki M, Matsuda S, Imachi T, Miyoshi Y, Hikishima M, Katoh Y, Ota M, Shoji M, Matsuoka A, Shinohara I (2018c) The plasma wave experiment (PWE) on board the Arase (ERG) satellite. Earth Planets Space 70:86. https://doi.org/10.1186/s40623-018-0842-4

Katoh Y, Omura Y (2007) Computer simulation of chorus wave generation in the Earth's inner magnetosphere. Geophys Res Lett. https://doi.org/10.1029/2006gl028594

Katoh Y, Kojima H, Hikishima M, Takazhima T, Asamura K, Miyoshi Y, Kasahara S, Mitani T, Higashio N, Matsuoka A, Ozaki M, Yagitani S, Yokota S, Matsuda S, Kitahara M, Shinohara I (2018) Software-type wave–particle interaction analyzer on board the Arase satellite. Earth Planets Space 70:4. https://doi.org/10.1186/s40623-017-0771-7

Kazama Y, Wang BJ, Wang SY, Ho PTP, Tam SWY, Chang TF, Chiang CY, Asamura K (2017) Low-energy particle experiments-electron analyzer (LEPe) onboard the Arase spacecraft. Earth Planets Space 69:165. https://doi.org/10.1186/s40623-017-0748-6

Kumamoto A, Tsuchiya F, Kasahara Y, Kasaba Y, Kojima H, Yagitani S, Ishisaka K, Imachi T, Ozaki M, Matsuda S, Shoji M, Matsuoka A, Katoh Y, Miyoshi Y, Obara T (2018) High frequency analyzer (HFA) of plasma wave experiment (PWE) onboard the Arase spacecraft. Earth Planets Space 70:82. https://doi.org/10.1186/s40623-018-0854-0

Ma Q, Li W, Chen L, Thorne RM, Angelopoulos V (2014) Magnetosonic wave excitation by ion ring distribution in the Earth's magnetosphere. J Geophys Res. https://doi.org/10.1002/2014gl061414

Matsuda S, Kasahara Y, Kojima H, Kasaba Y, Yagitani S, Ozaki M, Imachi T, Ishisaka K, Kumamoto A, Tsuchiya F, Ota M, Kurita S, Miyoshi Y, Hikishima M, Matsuoka A, Shinohara I (2018) Onboard software of plasma wave experiment aboard Arase: instrument management and signal processing of wave form capture/onboard frequency analyzer. Earth Planets Space 70:75. https://doi.org/10.1186/s40623-018-0838-0

Matsuoka A, Teramoto M, Nomura R, Nose M, Fujimoto A, Tanaka Y, Shinohara M, Nagatsuma T, Shiokawa K, Obana Y, Miyoshi Y, Mita M, Takashima T, Shinohara I (2018) The Arase (ERG) magnetic field investigation. Earth Planets Space 70:43. https://doi.org/10.1186/s40623-018-0800-1

Mauk BH, Fox NJ, Kanekal SG, Kessel RL, Sibeck DG, Ukhorskiy A (2013) Science objectives and rationale for the radiation belt storm probes mission. Space Sci Rev. https://doi.org/10.1007/s11214-012-9908-y

McIlwain CE (1961) Coordinates for mapping the distribution of magnetically trapped particles. J Geophys Res. https://doi.org/10.1029/jz066i011p03681

Mitani T, Takashima T, Kasahara S, Miyake W, Hirahara M (2018) High-energy electron experiments (HEP) aboard the ERG (Arase) satellite. Earth Planets Space 70:77. https://doi.org/10.1186/s40623-018-0853-1

Miyoshi Y, Kataoka R (2005) Ring current ions and radiation belt electrons during geomagnetic storms driven by coronal mass ejections and corotating interaction regions. Geophys Res Lett. https://doi.org/10.1029/2005GL024590

Miyoshi Y, Morioka A, Obara T, Misawa H, Nagai T, Kasahara Y (2003) Rebuilding process of the outer radiation belt during the November 3: 1993, magnetic storm—NOAA and EXOS-D observations. J Geophys Res. https://doi.org/10.1029/2001ja007542

Miyoshi Y, Sakaguchi K, Shiokawa K, Evans D, Albert J, Conners M, Jordanova V (2008) Precipitation of radiation belt electrons by EMIC waves, observed from ground and space. Geophys Res Lett. https://doi.org/10.1029/2008GL035727

Miyoshi *et al. Earth, Planets and Space* (2018) 70:101

Page 13 of 13

Miyoshi Y, Ono T, Takashima T, Asamura K, Hirahara M, Kasaba Y, Matsuoka A, Kojima H, Shiokawa K, Seki K, Fujimoto M, Nagatsuma T, Cheng CZ, Kazama Y, Kasahara S, Mitani T, Matsumoto H, Higashio N, Kumamoto A, Yagitani S, Kasahara Y, Ishisaka K, Blomberg L, Fujimoto A, Katoh Y, Ebihara Y, Omura Y, Nose Hori T, Miyashita Y, Tanaka Y-M, Segawa, ERG working group (2012) The energization and radiation in geospace (ERG) project. In: Summers D, Mann IR, Baker DN, Schulz M (eds) Dynamics of the Earth's radiation belts and inner magnetosphere. American Geophysical Union, Washington. https://doi.org/10.1029/2012gm001304

Miyoshi Y, Kataoka R, Ebihara Y (2016) Flux enhancement of relativistic electrons associated with substorms. In: Balasis G, Daglis IA, Mann IR (eds) Waves, particles, and storms in geospace. Oxford Press, Oxford, pp 333–353

Miyoshi Y, Hori T, Shoji M, Teramoto M, Chang T-F, Segawa T, Umemura N, Matsuda S, Kurita S, Keika K, Miyashita Y, Seki K, Tanaka Y, Nishitani N, Kasahara S, Yokota S, Matsuoka A, Kasahara Y, Asamura K, Takashima T, Shinohara I (2018) The ERG science center. Earth Planets Space 70:96. https://doi.org/10.1186/s40623-018-0867-8

Nagai T (1988) Space weather forecast: prediction of relativistic electron intensity at synchronous orbit. Geophys Res Lett 15:425

Nakamura Y et al (2018) Exploration of energization and radiation in geospace (ERG): challenges, development, and operation of satellite system. Earth Planets Space. https://doi.org/10.1186/s40623-018-0863-z

Nose M et al (2005) Overwhelming O^+ contribution to the plasma sheet energy density during the October 2003 superstorm: geotail/EPIC and IMAGE/LENA observations. J Geophys Res 110:A09S24. https://doi.org/10.1029/2004ja010930

Omura Y, Hikishima Katoh Y, Summers D, Yagitani S (2009) Nonlinear mechanisms of lower-band and upper-band VLF chorus emissions in the inner magnetosphere. J Geophys Res. https://doi.org/10.1029/2009JA014206

Ozaki M, Yagitani S, Kojima H, Kasahara Y, Kasaba Y, Matsuoka A, Sasaki T, Yumoto T (2018) Magnetic search coil (MSC) of plasma wave experiment (PWE) aboard the Arase (ERG) satellite. Earth Planets Space 70:76. https://doi.org/10.1186/s40623-018-0837-1

Reeves GD, McAdams KL, Friedel RHW, O'Brien TP (2003) Acceleration and loss of relativistic electrons during geomagnetic storms. Res Lett, Geophys. https://doi.org/10.1029/2002GL016513

Reeves GD, Spence HE, Henderson MG, Morely SK, Friedel RHW, Funsten HO, Baker DN, Kanekal SG, Blake JB, Fennell JF, Claudepierre SG, Thorne RM, Turner DL, Kletzing CA, Kurth WS, Larson BA, Niehof JT (2013) Electron acceleration in the heart of the Van Allen radiation belts. Science. https://doi.org/10.1126/science.1237743

Saito S, Miyoshi Y, Seki K (2012) Relativistic electron microbursts associated with whistler chorus rising tone elements: GEMSIS-RBW simulations. J Geophys Res. https://doi.org/10.1029/2012JA018020

Seki K, Miyoshi Y, Ebihara Y, Katoh Y, Amano T, Saito S, Shoji M, Nakamizo A, Keika K, Hori T, Nakano S, Watanabe S, Kamiya K, Takahashi N, Omura Y, Nose M, Fok MC, Tanaka T, Ieda A, Yoshikawa A (2018) Theory, modeling, and integrated studies in the Arase (ERG) project. Earth Planets Space 70:17. https://doi.org/10.1186/s40623-018-0785-9

Shiokawa K, Katoh Y, Hamaguchi Y, Yamamoto Y, Adachi T, Ozaki M, Oyama SI, Nose M, Nagatsuma T, Tanaka Y, Otsuka Y, Miyoshi Y, Kataoka R, Takagi Y, Takeshita Y, Shinbori A, Kurita S, Hori T, Nishitani N, Shinohara I, Tsuchiya F, Obana Y, Suzuki S, Takahashi N, Seki K, Kadokura A, Hosokawa K, Ogawa Y, Connors M, Ruohoniemi JM, Engebretson M, Turunen E, Ulich T, Manninen J, Kurkin V, Oinats A, Pashinin A, Vasilyev R, Rakhmatulin R, Bristow W, Karjala M (2017) Ground-based instruments of the PWING project to investigate dynamics of the inner magnetosphere as subauroral latitudes as a part of the ERG-ground coordinated observation network. Earth Planets Space 69:160. https://doi.org/10.1186/s40623-017-0745-9

Shprits YY, Elkington SR, Meredith NP, Subbotin DA (2008a) Review of modeling of losses and sources of relativistic electrons in the outer radiation belt I: radial transport. J Atm Solar Terr Phys 70:1679–1693

Shprits YY, Subbotin DA, Meredith NP, Elkington SR (2008b) Review of modeling of losses and sources of relativistic electrons in the outer radiation belt II: local acceleration and loss. J Atmos Solar Terr Phys 70:1694–1713

Summers D, Thorne RM, Xiao F (1998) Relativistic theory of wave-particle resonant diffusion with application to electron acceleration in the magnetosphere. J Geophys Res 103:20487–20500

Takashima T, Ogawa E, Asamura K, Hikishima M (2018) Design of mission network system with SpaceWire for scientific payloads onboard the Arase spacecraft. Earth Planet Space, https://doi.org/10.1186/s40623-018-0839-z

Thorne RM (2010) Radiation belt electrons: The importance of wave–particle interactions. Res Lett, Geophys. https://doi.org/10.1029/2010GL044990

Turner DL, Morley SK, Miyoshi Y, Ni B, Huang C-L (2012) Outer belt flux dropouts: current understanding and unresolved questions. In: Summers D, Mann IR, Baker DN, Schulz M (eds) Dynamics of the Earth's radiation belts and inner magnetosphere. American Geophysical Union, Washington. https://doi.org/10.1029/2012gm001310

Yokota S, Kasahara S, Mitani T, Asamura K, Hirahara M, Takashima T, Yamamoto K, Shibano Y (2017) Medium-energy particle experiments-ion mass analyzer (MEP-i) onboard ERG (Arase). Earth Planets Space 69:172. https://doi.org/10.1186/s40623-017-0754-8